J. Wind Eng. Ind. Aerodyn. 135 (2014) 105–117

Contents lists available at ScienceDirect

Journal of Wind Engineering and Industrial Aerodynamics

journal homepage: www.elsevier.com/locate/jweia

Experimental investigation of the slipstream development around a container freight train using a moving model facility

David Soper*, Chris Baker, Mark Sterling

Birmingham Centre for Railway Research and Education, School of Civil Engineering, University of Birmingham, UK

ARTICLE INFO

Article history:
Received 20 June 2014
Received in revised form
8 September 2014
Accepted 6 October 2014
Available online 7 November 2014

Keywords:
Aerodynamics
Freight train
Slipstream
Experimental study
Model-scale

ABSTRACT

Increases in the volume of trade within the UK rail freight industry have led to proposed increases in freight train speeds. There is a concern that the unsteady slipstream created around a moving freight train could have implications on efficiency and the safety of passengers waiting on platforms or trackside workers. This paper describes a series of moving model-scale experiments conducted at the University of Birmingham's TRAIN rig facility. Experiments were undertaken to assess the slipstream development of a container freight train and draw conclusions on flow characteristics. In this paper the term 'freight train' refers to a series of flatbed wagons loaded with ISO standard shipping containers hauled by a Class 66 locomotive. In-depth analysis of slipstream velocity and static pressure ensemble average results at train side and above the roof identified a series of key flow regions. Results within the boundary layer region exhibit an influence from container loading configuration. Slipstream magnitudes are larger than typical high speed passenger train results, which it is suggested is related to the vehicle shape. The effect of train length and train speed was also considered. A detailed analysis of the nature of slipstream velocity components in specific flow regions is investigated, and conclusions drawn on characteristic patterns and factors influencing possible safety issues. The analysis highlighted differences created through decreased container loading efficiencies, creating increased boundary layer growth with a larger displacement thickness with higher turbulence intensities. Integral time and length scales calculated through autocorrelation indicate that proposed limits of human instability are exceeded for the container freight train with a lower loading efficiency. Overall the results from this paper offer for the first time a definitive experimental study on container freight slipstream characteristics, allowing the nature of the flow field around freight trains to be understood in far greater detail than before.

1. Introduction

The UK rail freight industry is a growing sector with increasing volumes of international trade coupled with a gradual transfer from road to rail transportation. The UK government has set aims to double the volume of rail freight cargo on the UK rail network by 2030 (Department for Transport DfT. Delivering a Sustainable Railway, 2007). Efficiency studies into increased volumes of freight trains within an already overstretched network, primarily focused on passenger transportation, recommend building new and reopening closed railway lines, while developing faster and longer trains (Woodburn, 2008). However, infrastructure developments are expensive and would take several years to complete. Capacity could be increased by lengthening freight trains; however, this may lead to slower trains, due to locomotive power, thus creating further congestion within the rail network (Frost et al., 2012). The final option to increase freight operational speeds would be simpler to implement and lead to increased route capacity. This however has implications on efficiency and safety, as the movement of a vehicle causes deformation in the surrounding air, creating transient aerodynamic effects.

The airflow around a moving vehicle is called a slipstream, characterised by a highly turbulent non-stationary region of air (Baker et al., 2001). Induced slipstream forces can interact with trackside objects, potentially destabilising such objects and people. In the last forty years there have been twenty six train slipstream incidents on the UK rail network, the majority caused by freight trains. In one incident a braked pushchair was drawn by the slipstream 3 m towards a freight train, hitting the moving train and thrown across the platform into two passengers (Temple and Johnson, 2008). Knowledge of slipstream velocity and pressure magnitudes is therefore important in the authorisation of increased train speeds and development of new trains (Baker et al., 2013).

Concerns over the possibility of slipstream induced incidents have led to a number of studies into the effects of slipstreams,

* Correspondence to: Birmingham Centre for Railway Research and Education, School of Civil Engineering, University of Birmingham, Edgbaston, Birmingham B15 2TT, UK.
E-mail address: d.soper@bham.ac.uk (D. Soper).

http://dx.doi.org/10.1016/j.jweia.2014.10.001

Notation

C_p	coefficient of pressure
N	number of independent runs undertaken to create the ensemble average
R	gas constant (J/kg K)
T_{room}	room temperature (K)
U	ensemble longitudinal component of slipstream velocity, normalised by train speed
V	ensemble lateral component of slipstream velocity, normalised by train speed
V_{train}	train speed (m/s)
W	ensemble vertical component of slipstream velocity, normalised by train speed
p_0	ambient pressure (Pa)
u	ensemble longitudinal component of slipstream velocity (m/s)
v	ensemble lateral component of slipstream velocity (m/s)
w	ensemble vertical component of slipstream velocity (m/s)
x	distance along the track measured from vehicle front (m)
y	distance normal to the track measured from the centre of the track (m)
z	distance in the vertical direction measured from the top of the rail (m)
ν	kinematic viscosity (m^2/s)
ρ	density of air (kg/m^3)

mainly for high speed passenger trains (Baker et al., 2001, 2013; Pope, 2006; Sterling et al., 2008). Results show the flow can be divided into a number of regions along the train – the upstream/nose region characterised by a velocity peak; the boundary layer region characterised by a boundary layer growth along the length of the train; a tail/near wake region shown to be highly turbulent with a series of shear layer separations or periodic longitudinal vortices and a far wake region exhibiting gradual decay of slipstream velocities. Individual results were shown to be highly variable, as the flow is dominated by large scale turbulent structures, thus the technique of ensemble averaging is required when studying train slipstreams (Sterling et al., 2008). Results from these and other studies have led to the development of the Technical Specifications for Interoperability (TSI); a series of laws on train aerodynamics giving limiting values for slipstream velocities, allowing for interoperability of trains across national boundaries in Europe (Technical Specifications for Interoperability. Commission, 2008). Although some freight research has been included in these studies, a thorough study of freight slipstream development and appropriate guidelines written in relation to rail freight is yet to be undertaken.

This paper will present and analyse the results of a series of experiments to assess slipstream development of a container freight train that were carried out as part of the first author's doctoral study (Soper, 2014). Results from a series of open air moving model-scale experiments undertaken at the University of Birmingham's TRAIN (TRansient Aerodynamic INvestigation) rig facility in Derby are presented and analysed. The experiment facility and model are described in Section 2.1. The adopted coordinate system and experiment methodology are discussed in Section 2.2. Section 2.3 introduces the measuring instrumentation and method of ensemble analysis. The experimental results and analysis are presented in Section 3 for coefficient of pressure (Section 3.1), normalised ensemble longitudinal component of velocity U (Section 3.2) and normalised ensemble lateral and vertical components of velocity V and W (Section 3.3). Section 4 presents a discussion of the various analysis techniques previously employed in high speed passenger train studies and the results when these methods were applied for freight slipstreams. Finally, Section 5 presents conclusions drawn in this model-scale study.

2. Experimental methodology

2.1. TRAIN rig and experiment model

The TRAIN rig is a purpose built testing facility for examining the transient aerodynamics of moving vehicles (Baker et al., 2001). It consists of three 150 m long tracks along which reduced scale vehicles can be propelled at speeds up to 75 m/s. The TRAIN rig offers the possibility to measure slipstream velocities, static pressure pulses and pressures acting on the train or trackside structures in a 12 m long open air test section (Baker et al., 2014). The effects of crosswinds at various yaw angles and ground simulations can also be modelled using a purpose built 6.35 m long crosswind generator (Dorigatti, 2013; Soper et al., 2014). A 23 m long tunnel is also installed for the measurement of vehicle aerodynamics in tunnel confines. The advantage of using a moving model rig over a typical stationary wind tunnel is the ability to correctly simulate relative motion between the vehicle and the ground/structures or crosswind simulation.

Models are accelerated using a pre-tensioned elastic bungee cord system, ensuring the rate of acceleration occurs very rapidly; thus the model is travelling at the specified testing speed within a 50 m firing section. Once in motion the model is free from any propulsion devices, allowing free motion with minimal constraints on model design. However, due to aerodynamic drag and friction, a small decrease in vehicle speed is created between the firing and braking section. For the models tested in this experimental campaign, an average speed decrease of 1 m/s^2 has been estimated for an average train speed of 20 m/s through the open air testing section. Following the 50 m test section, the model is decelerated using a friction device in a 50 m braking section. The firing, open air testing and brake zones are shown in Fig. 1.

A 1/25th scale moving model was developed to simulate container loading configurations seen at full-scale. Unlike focusing on a specific high speed passenger train, the term 'freight train' applies to many different train types (e.g. containers, tankers, mineral wagons etc.). For this study the term 'freight train' refers to a series of flatbed wagons loaded with International Shipping Organisation (ISO) standard shipping containers hauled by a Class 66 locomotive. Container freight is one of the largest sectors of freight transported in the UK and the choice for this study offers relative ease for modelling purposes. An existing Class 66 model was modified to include a long flat plate to simulate four/eight FEA type B flatbed wagons, with bogies modelled using balsa wood, shown in Fig. 2. The model is mounted on a specially designed chassis and trailing wheel system, designed to spread model weight out evenly, providing stability and a structure by which to fire/brake the model. The Class 66 model is mounted onto the chassis (Fig. 2a)), while four/eight (depending on model length) sets of trailing wheels are attached at varying distances along the flat plate (Fig. 2b)). The chassis and trailing wheels axle plate, onto which the wheel is mounted, extends below the radius of the wheel and the head of the rail to an L-shaped skid plate (Fig. 2b)),

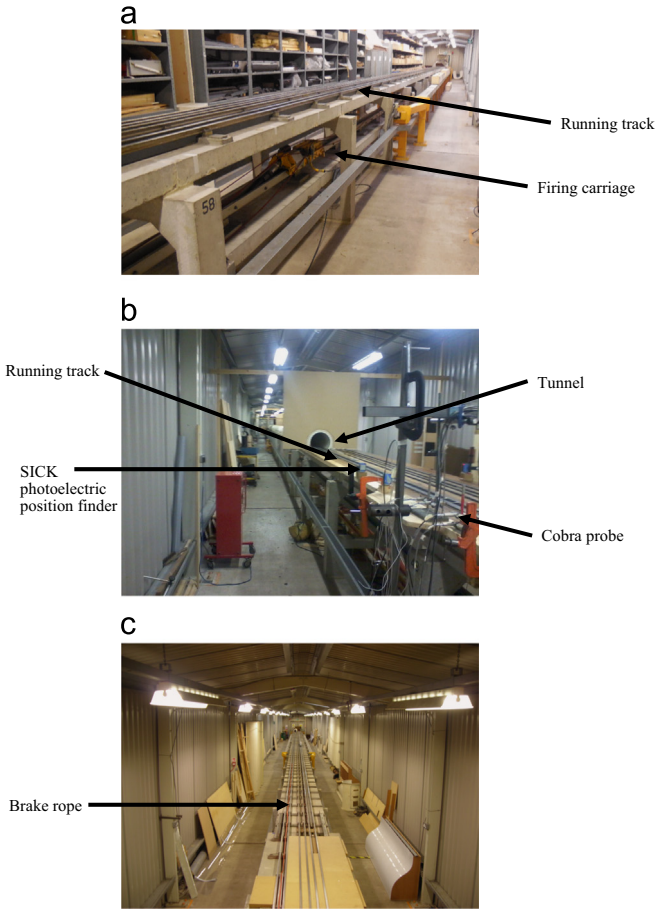

Fig. 1. The TRAIN rig facility. The images show (a) the firing, (b) open air test and (c) braking zones respectively.

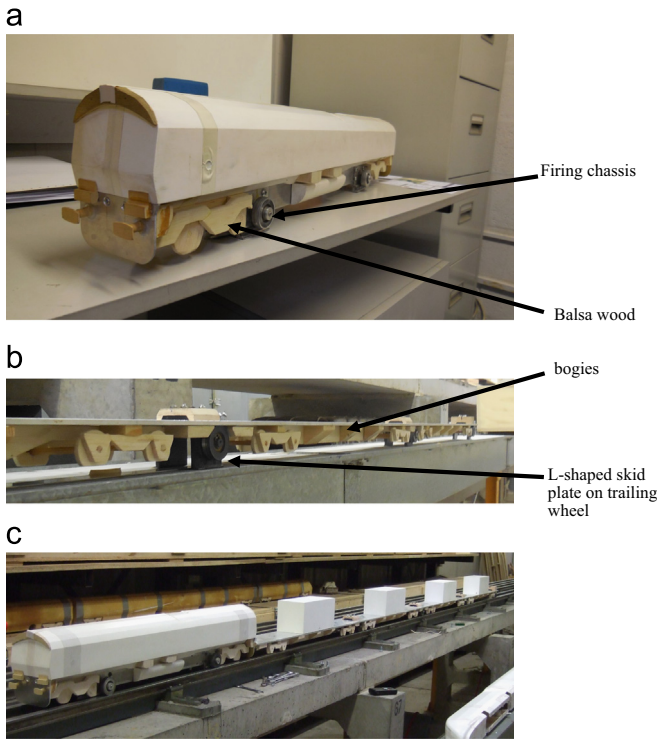

Fig. 2. The TRAIN rig freight model. The freight train consists of (a) a Class 66 locomotive and (b) a series of flatbed wagons, with balsa wood bogies (also shown are the TRAIN rig trailing wheel system). Image (c) is the 4 wagon freight train with loading consist 3 attached (see Fig. 5).

allowing the train to move along the track in a longitudinal direction but negating lateral and vertical motion. Figs. 3 and 4 show dimensions for the Class 66 and a twin set of FEA type B wagons respectively; dimensions given in terms of a full-scale train.

There are twelve scale 6.10 m containers, and eight 12.19 m containers arranged in various configurations to represent a cross section of different container loading efficiencies and provide data for comparison to full-scale results; the loading configurations discussed within this study are shown in Fig. 5. For the 8 wagon train the loading configuration over the first 4 wagons is repeated. The container surfaces are simplified by neglecting a series of corrugations seen at full-scale; a simplification previously employed by Alam and Watkins (2007) and Hemida and Baker (2010) with satisfactory results.

A number of simplifications were made to conduct the slipstream experiments at model-scale. A freight train generally consists of a locomotive hauling a series of wagons; at model-scale a maximum of eight flatbed wagons are modelled, shorter than an average freight train length, to be within the working range of the elastic bungee cord acceleration system. Detailed components such as bogies are geometrically simplified and the experiment is conducted as an open track with no ballast shoulder modelled. Simplifications of a similar manner have been previously adopted for model-scale studies of high speed passenger trains (Baker et al., 2001; Sterling et al., 2008). Throughout this model-scale study a train speed $V_{train}=20\pm0.5$ m/s (45 ± 1 mph) is chosen; less than the maximum UK freight operational speed of 33.5 m/s (75 mph). The reduced train speed is necessary to be within the working range of the measuring instrumentation (Section 2.3). The corresponding Reynolds number is 2.2×10^5 based on V_{train} and the Class 66 height (156 mm at 1/25 scale). Previous passenger studies have shown despite relatively low Reynolds numbers for model-scale experiments good agreement is found with full-scale experimental results, indicating a lack of sensitivity to Reynolds number effects (Baker, 2010; Muld, 2012). Reynolds number sensitivity is discussed further in Section 3.2 by comparing results for differing train speeds.

2.2. Coordinate system and measuring positions

A coordinate system is defined as in Fig. 6 such that the x-axis is aligned in the direction of travel, with the origin taken to be when the train nose passes the measuring point. The y-axis is the horizontal plane perpendicular to the track direction, measured from the centre of track and the z-axis is in the vertical direction measured from the top of the rail. Slipstream velocities and static pressure are measured at a series of fundamental positions away from the train side and roof in line with previous studies (Baker et al., 2001; Gil et al., 2008). Fig. 6 and Table 1 show the measuring positions, given in full-scale dimensions. It should be noted that due to time constraints it was not possible to carry out experiments for each loading configuration at each measuring position.

2.3. Measuring instrumentation and ensemble analysis

Slipstream velocities and static pressure were measured using Cobra probes (TFI, Turbulent flow instrumentation, 2011). Cobra Probes are four-hole pressure probes capable of measuring three components of velocity and the local static pressure in real time. The probes are calibrated by the manufacturer, with an accuracy of ±0.5 m/s, ±5 Pa and $\pm1^\circ$ for velocity, static pressure and direction respectively. A drawback to the probe is a $\pm45^\circ$ cone of acceptance, limiting the range of flow detection. For flow outside the cone of acceptance, the data is replaced by a zero (referred to as a 'dropout'). Dropouts were highest around the Class 66 nose due to flow

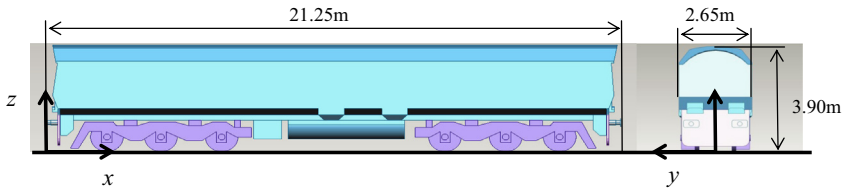

Fig. 3. Dimensions of the Class 66 locomotive. All dimensions are given in terms of a full-scale train.

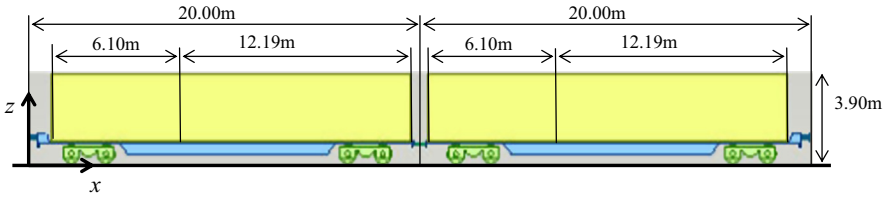

Fig. 4. Dimensions for a FEA type B wagon twin set. All dimensions are given in terms of a full-scale train.

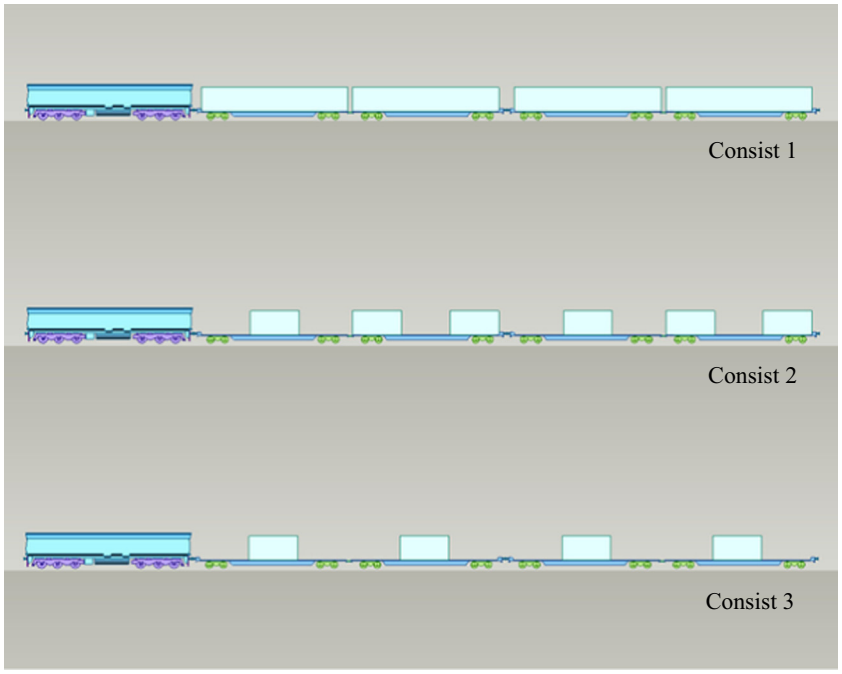

Fig. 5. The container loading configurations used in this paper. Consist 1, 2 and 3 have 100%, 50% and 33% loading efficiencies respectively. The model train with consist 3 is also shown in Fig. 2c).

reversal. A sampling frequency of 2500 Hz was chosen to avoid signal aliasing and with a train speed of $V_{train}=20\pm0.5$ m/s provided measurements every 8 mm along the TRAIN rig model, corresponding to every 0.2 m at full-scale.

Sterling et al. (2008) noted that time histories for individual runs are highly variable and thus the method of ensemble averaging must be employed. European TSI standards state an experiment should be conducted at least 20 times to validate results (Technical Specifications for Interoperability. Commission, 2008). The method assumes a signal is measured '*N*' times in respect to an axial coordinate position (for this study $x=0$). To account for the small differences in train speed which may occur during each run, and hence cause the ensemble to be out of alignment with increasing values of x, individual runs were resampled with respect to the nominal train speed $V_{train}=20$ m/s, allowing an ensemble to be created with respect to a common distance axis. The ensemble average is then calculated by taking the average value of all runs at each increment in x. This method however has issues associated with the Cobra probe 'dropouts'. At the train nose it is possible to observe a region where no data is recorded for all runs, and in the boundary layer sections of dropouts are associated with the highly turbulent nature of this region. To eliminate this issue zero data is disregarded in the ensemble calculation, therefore a moving ensemble size at each increment in x is employed. To create ensemble averages in line with TSI standards, with a mean ensemble size of 20, a total of 25 repeats were undertaken for each container loading configuration.

Ensemble averages for slipstream velocities and static pressure are presented in terms of non-dimensionalised coefficients (Eqs. (1)–(4)),

$$U(x)=\frac{u(x)}{V_{train}} \tag{1}$$

$$V(x)=\frac{v(x)}{V_{train}} \tag{2}$$

$$W(x)=\frac{w(x)}{V_{train}} \tag{3}$$

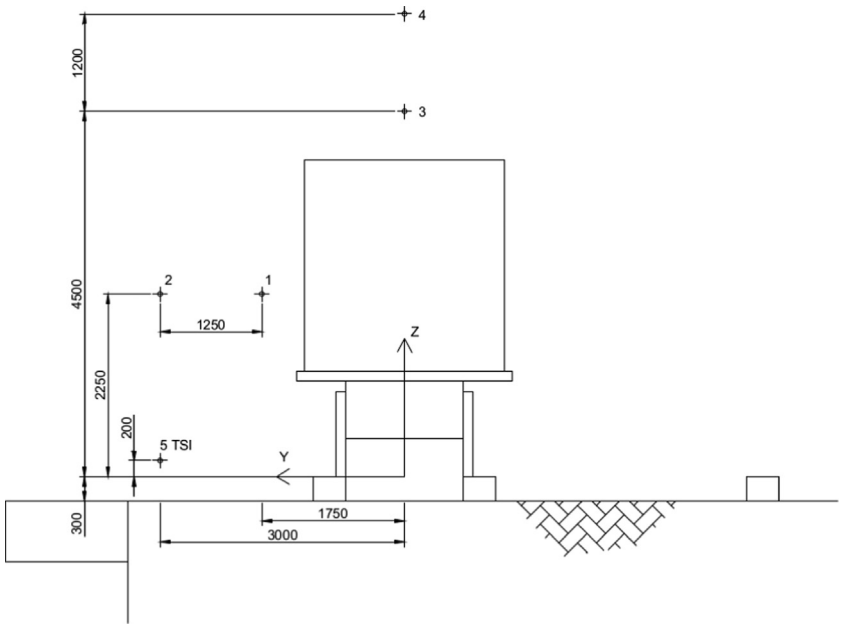

Fig. 6. A schematic of the coordinate system and Cobra probe measuring positions at the TRAIN rig for the freight slipstream experiments (Table 1). The *x*-direction in this figure is in the direction of vehicle motion, in this case into the paper.

Table 1
The measuring positions and the loading configurations tested at each position for the model-scale freight experiments conducted at the TRAIN rig facility.

Probe number	Measuring positions		Consists tested	
	Height (mm)	Distance from track centre (mm)	4 Wagon train	8 Wagon train
1	2250	1750	1, 2, 3	1, 2, 3
2	2250	3000	1, 2, 3	1, 2, 3
3	4500	0	1, 2, 3	1, 2, 3
4	5700	0	3	1, 2, 3

$$C_p(x) = \frac{p(x) - p_0}{0.5\rho V_{train}^2} \quad (4)$$

where u, v and w are the ensemble longitudinal, lateral and vertical components of velocity respectively. U is the normalised ensemble longitudinal component of velocity, V is the normalised ensemble lateral component of velocity, W is the normalised ensemble vertical component of velocity and C_p is the coefficient of pressure. p_0 is defined as the ambient reference pressure, measured by a GBP3300 Digital Barometer, and ρ is the density of air calculated using the gas constant $R=287$ (J/kg K) and the room temperature T_{room}, measured by a Oregon Scientific BAR208HGA weather station.

The model speed was measured using a series of opposing SICK photoelectric position finders at trackside. The position finders were separated by 1 m and 2 m about a central lateral position located at $x=0$, in line with the Cobra probe measuring head. The train speed is calculated based on the time taken for the model to break both beams, to an accuracy of ± 0.1 m/s.

3. Slipstream ensemble analysis of model-scale experimental data

3.1. Coefficient of pressure

Fig. 7 illustrates the coefficient of pressure C_p for the 8 wagon train for consists 1 to 3 measured at fundamental positions 1 to 4 at train side and above the roof. As in previous studies the flow can be split into a number of key regions; upstream and nose ($x \leq 18.75$ m), boundary layer (18.75 m $\leq x \leq$ 181.25 (train end)), tail and wake ($181.25 \leq x$) (Baker et al., 2001). As the leading vehicle of the train is always the same (Class 66 locomotive) the upstream and nose regions are essentially the same for each consist, with small differences due to statistical run to run variability, as discussed in Section 2. Ahead of the train nose there is a positive peak in C_p, followed by a negative peak in C_p following the passage of the train nose. It should be noted that between the positive and negative C_p peaks there is a section of no data, as the highly three-dimensional flow is beyond the $\pm 45^\circ$ cone of influence capability of the Cobra probe.

The train nose passes the measuring point when C_p passes through zero between the positive and negative peaks. The nose region extends from ± 18.75 m at full-scale. The magnitudes of peaks in this region are much higher than those seen previously in passenger train slipstream studies (Baker et al., 2001; Hemida et al., 2010). However, it was shown in Baker et al. (2014) that the Class 66 created much greater nose peak magnitudes than either a Class 390 or Class 158 passenger train on trackside structures. It is suggested that the magnitude of C_p in this region is closely related to the shape of the train nose, which for the Class 66 is highly bluff.

In the boundary layer region (18.75 m $\leq x \leq$ 181.25 m (train end)) differences in container loading efficiency can clearly be seen. For consist 1 C_p stabilises to zero following the nose region, with minor transients due to the small gaps between the loaded containers, similar to a passenger train with inter-carriage gaps (Hemida et al., 2010). For consists 2 and 3 the influence of larger spaces between loaded containers creates a series of positive and negative peaks, similar to the nose region, about the lead face of each container. At the rear face of the container a smaller negative peak is observed. Between loaded containers C_p increases to the positive peak seen before the face of the following container. The magnitude of container leading face peaks are affected by space size between containers. The influence of wagon design in relation to C_p is apparent for consist 2. The FEA type B wagon is designed as a twin set wagon, i.e. two wagons constantly joined together, with the braking mechanisms situated at the outer end of each twin wagon set, thus the space between two wagons in a twin is smaller than the space between two twin sets. For consist 2 the influence of the larger space between two wagon sets creates a

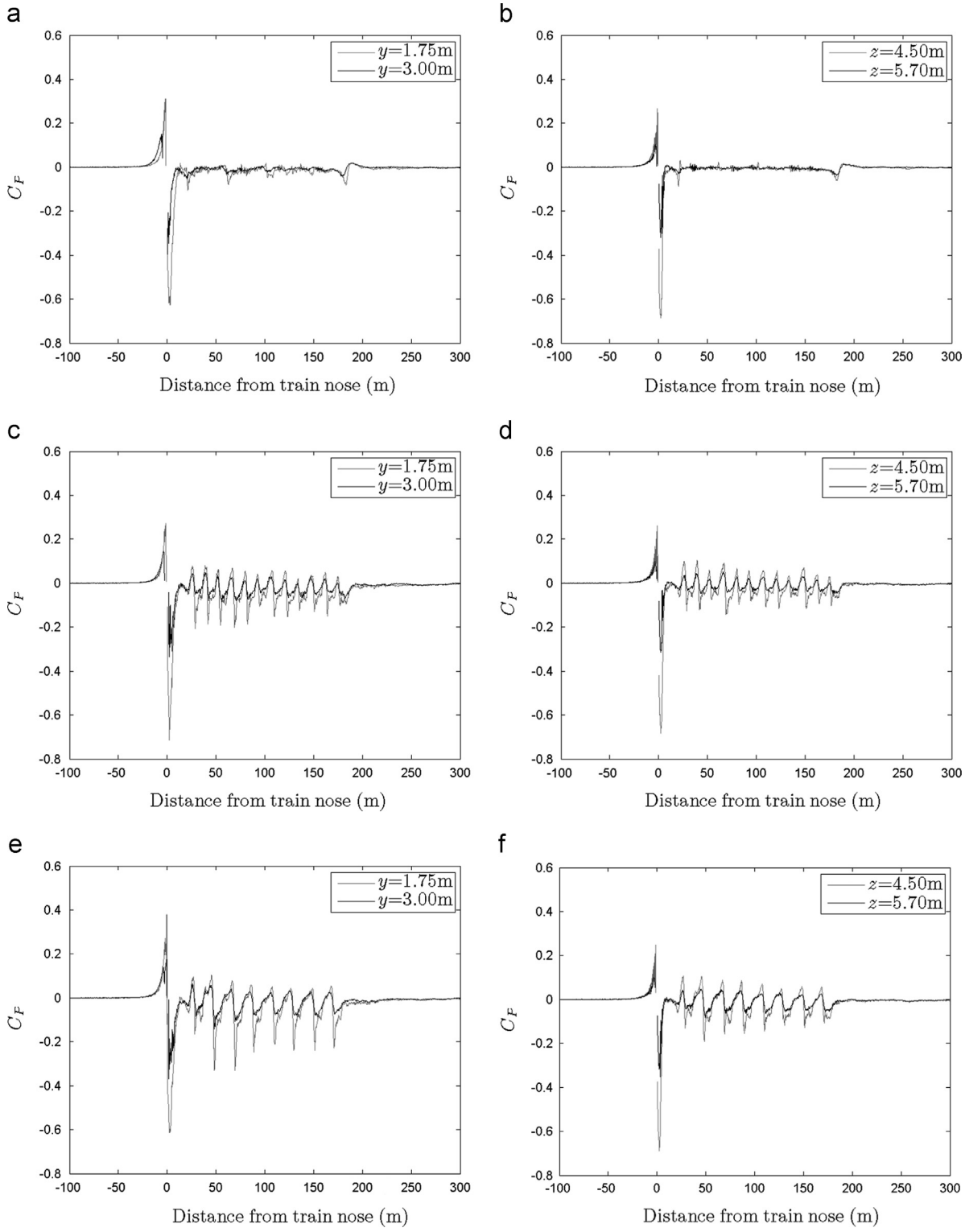

Fig. 7. The coefficient of pressure C_p, for freight consists 1 to 3 on the 8 wagon train. Measurements are made at train side at a height of $z=2.25$ m at distances $y=1.75$ m and $y=3$ m from the centre of track, and above the train roof for heights $z=4.5$ m and $z=5.7$ m at a position of 0 m from the centre of track. a) Consist 1 probes 1 and 2; b) Consist 1 probes 3 and 4; c) Consist 2 probes 1 and 2; d) Consist 2 probes 3 and 4; e) Consist 3 probes 1 and 2 and f) Consist 3 probes 3 and 4.

larger disturbance in C_p within the boundary layer in comparison to the space between wagons in a twin set (Fig. 7).

In the tail region a reversal of the nose region is witnessed, with a negative peak followed by a positive peak, however much smaller in magnitude. The characteristic tail region flow pattern has previously been observed in passenger studies, with a magnitude of similar order to passenger nose region peaks. It is suggested that the differences between passenger and freight tail regions are due to tail shape. The tail feature is also affected by container loading. For consists 1 and 2, with a loaded container close to the train tail, the tail feature is more defined than for consist 3 without. In the wake region C_p stabilises to zero within

20 m of the train tail for all consists. As the measuring distance from centre of track is increased the magnitude of C_p decreases for all loading configurations.

A similar series of flow regions to the train side are witnessed above the train roof. The characteristic nose flow pattern is observed, however with different maxima to those at a similar distance from train side. It is considered that differences between positive C_p peak magnitudes above the train roof and train side are related to the concave Class 66 nose shape and hooded section (Fig. 2a)). In the boundary layer region the characteristic flow patterns at container lead faces observed at train side are seen above the train roof, however with a smaller magnitude. As the

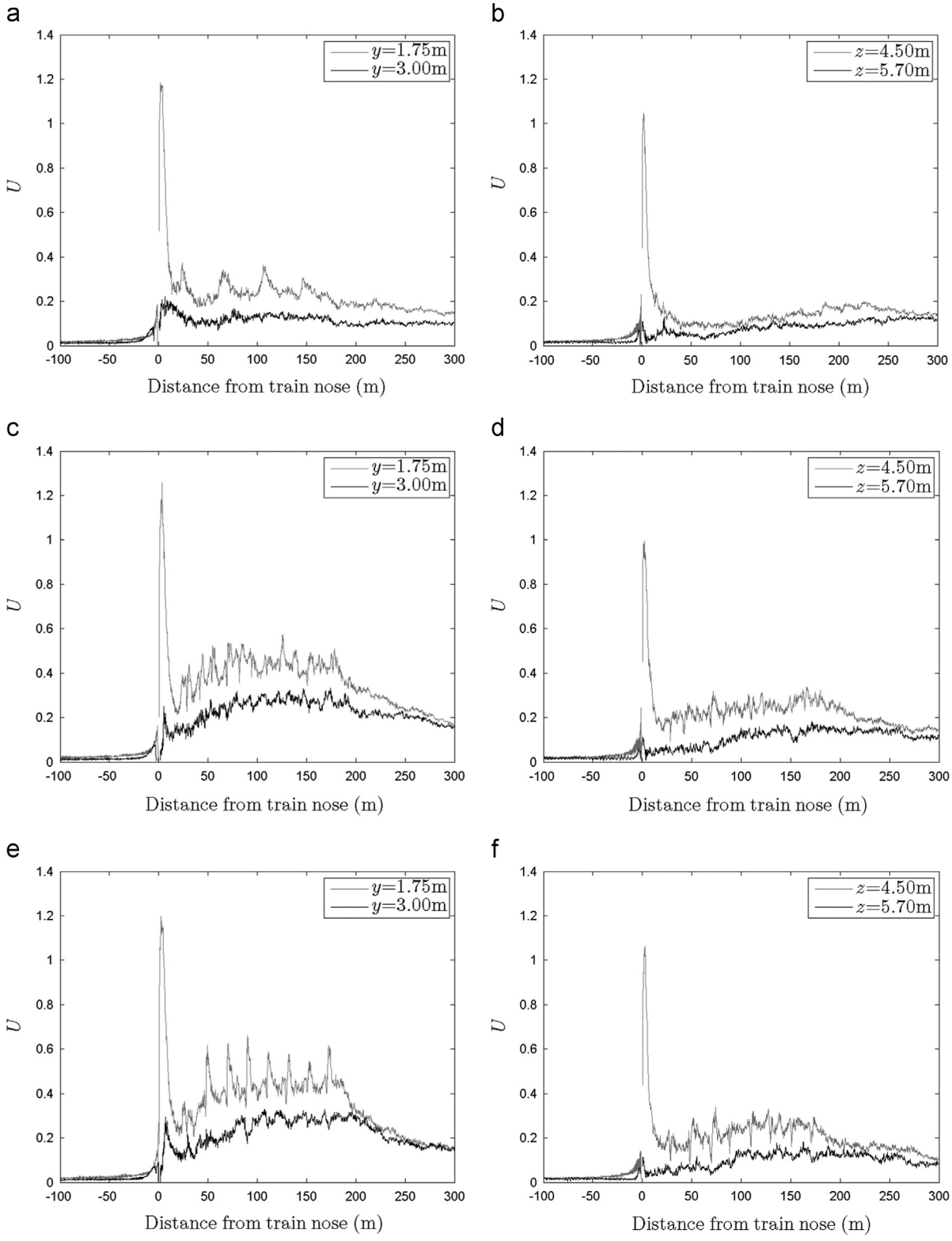

Fig. 8. The normalised ensemble longitudinal component of velocity U for the 8 wagon train. Measurements are made at train side at a height of $z=2.25$ m at distances $y=1.75$ m and $y=3$ m from the centre of track, and above the train roof for heights $z=4.5$ m and $z=5.7$ m at a position of 0 m from the centre of track. a) Consist 1 probes 1 and 2; b) Consist 1 probes 3 and 4; c) Consist 2 probes 1 and 2; d) Consist 2 probes 3 and 4; e) Consist 3 probes 1 and 2 and f) Consist 3 probes 3 and 4.

measuring height is increased the magnitude of C_p decreases for all loading configurations.

3.2. Normalised ensemble longitudinal component of velocity U

Fig. 8 illustrates the corresponding normalised ensemble longitudinal component of velocity U for the 8 wagon train for consists 1 to 3, measured at fundamental probe positions 1 to 4. As discussed previously, it is clear to see the flow can be split into a number of key regions. In the nose region there is a peak in U corresponding to the difference between positive and negative C_p peaks. The velocity in this region reaches 120% of train speed at 1.75 m from centre of track (probe 1), much higher than previously witnessed in passenger studies (Baker, 2010), which as with C_p is related to Class 66 nose shape. The nose peak magnitude is dramatically affected by distance from train side. It is thought that due to flow shearing/separation at the Class 66 nose side edge there is flow acceleration close to train side in the region containing probe 1. As the distance from train side is increased the influence of the shearing/separation is reduced and so U is much lower and slipstream development rapidly forms into boundary layer growth. The nose region extends from $\pm$ 18.75 m at full-scale.

In the boundary layer region the difference in container loading configuration can clearly be seen. For consist 1 the boundary layer stabilises rapidly after the train nose due to relatively smooth train sides, exhibiting similar flow development to a passenger train with inter-carriage gaps (Hemida et al., 2010). For consists 2 and 3 the influence of larger spaces between loaded containers creates increasing velocities along the train length, indicating a thickening boundary layer along the train side. The influence of spaces between containers causes pulse peaks in U within the boundary layer following the leading faces of the containers. As with C_p, the space size between loaded containers affects pulse peak magnitudes. The influence of spaces between loaded containers leads to a greater magnitude of U within the boundary layer region, thus a thicker boundary layer developing quicker than for a loading configuration with fewer spaces between loaded containers.

In the tail region boundary layer growth ceases and U falls away into the wake. This differs to the tail region of a passenger train, where a large tail velocity peak is observed due to longitudinal helical vortex structures, however the measuring of which depends on the measuring position (Sterling et al., 2008; Baker, 2010). The lack of velocity peak at the tail of a freight train has been previously observed by Sterling et al. (2008); it was also noted that the tail peak for a passenger train was only visible when the vortex shedding was in phase with the side on which the measuring equipment was situated. Analysis to identify if a tail peak existed for each individual run was undertaken; however, as with previous research this tail peak was none existent for the TRAIN rig model freight train. Differences between slipstream development in passenger and freight tail regions are due to tail shape (Section 4). In the wake region U falls away at a similar rate for all probes. The influence of the train is still visible into the far wake at a distance of over twice the train length from the Class 66 nose. As measuring distance from the centre of track is increased the magnitude of U decreases for all loading configurations.

It is possible to assess the influence of train length on U by comparing results from the 4 and 8 wagon train, Fig. 9. For partially loaded consists on the shorter freight train, following the nose region the boundary layer is seen to continually grow, punctuated with pulse peaks relating to the change in C_p at container lead faces. The longer train witnesses similar boundary layer growth to a distance of 100 m after which boundary layer stability is observed, whereby although pulse peaks in U are witnessed at container lead faces the mean boundary layer velocity is relatively constant. Therefore, for partially loaded container freight consists with a loading efficiency of less than 50%, more than 4 wagons are needed to capture the transition between boundary layer growth and stability.

Fig. 10 shows a comparison of model-scale data recorded for the 4 wagon train with consist 3 at train speeds V_{train}=20 m/s and V_{train}=25 m/s. Good agreement is observed between normalised ensemble data at different train speeds, illustrating a linear relationship with respect to train speed for velocity data and a squared relationship for pressure data.

Fig. 8 also shows U for train consists 1 to 3 measured at probe positions above the train roof. In the nose region the peak in U corresponds to the difference between positive and negative C_p peaks. The velocity above the train roof reaches 100% of train speed, lower than recorded at train side but higher than previous passenger results (Baker et al., 2001). In the boundary layer region the effect of container loading configuration can be observed, however the effect is suppressed in comparison to train side. In previous passenger studies (Baker et al., 2001; Gil et al., 2008), measurements taken above the train roof exhibit lower values for U than those recorded at train side. The rate at which U increases is lower above the train roof than at train side for all consists, suggesting flow remains relatively close to the train roof with a smaller boundary layer thickness than witnessed at train side.

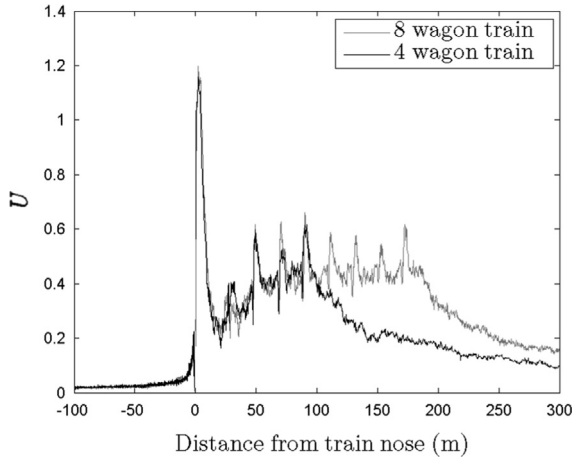

Fig. 9. The normalised ensemble longitudinal component of velocity U for the 4 wagon (black) and 8 wagon (grey) train with freight consist 3. Measurements are made at train side at a height of z=2.25 m at distance y=1.75 m from the centre of track.

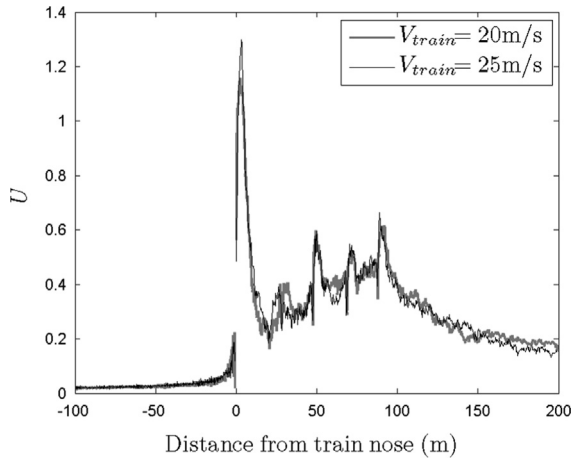

Fig. 10. The normalised ensemble longitudinal component of velocity U for the 4 wagon freight train with consist 3, at train speeds V_{train}=20 m/s (grey) and V_{train}=25 m/s (black). Measurements are made at train side at a height of z=2.25 m at distance y=1.75 m from the centre of track.

3.3. Normalised ensemble lateral and vertical components of velocity V and W

This study has, so far, discussed velocities in relation to U, the choice of which for analysis purposes reflects the methods of analysis in previous full-scale freight studies (Temple and Johnson, 2008; Sterling et al., 2008), to which comparisons are drawn. It will however be shown that for a container freight train it must be acknowledged that components V and W are not negligible as in passenger studies (Gil et al., 2008). Figs. 11 and 12 illustrate the normalised ensemble components of velocity V and W for the 8 wagon train with consists 1 and 3, measured at probe positions 1 to 4.

Previous passenger studies noted that except around the train nose and tail regions the overall magnitude is within 2% of the longitudinal velocity component U; suggesting lateral and vertical components of velocity are significantly small and below the performing range of the Cobra probe (Gil et al., 2008; Sterling et al., 2008). As discussed, consist 1 exhibits the closest relation to a passenger train. At train side and above train roof both V and W remain relatively constant, below the Cobra probe performing range except for the nose region where a positive then negative peak in velocity are observed. The nose region peaks are highly repeatable and exhibit a larger magnitude at train side than above the train roof, as seen for U. At train side, in general, the lateral component V has greater magnitude than the vertical component W, especially at the train nose and leading container faces. However, above the train roof the opposite occurs with a larger component of W than V. At the train nose or a container leading face a positive then negative peak is observed, i.e. flow away from the vehicle followed by flow towards the vehicle; a pattern characteristic of flow separation into a recirculation (Hemida and Baker, 2010). At train side this occurs in the lateral plane, creating greater increases in V than W, however above the train roof this process is dominated in the vertical plane, creating greater increases in W. As the loading efficiency is reduced it is possible to see similar pulse peaks at container faces in V and W as with U. At train side these peaks have a larger magnitude in V, to nearly 20% of train speed, whereas above train roof a larger magnitude in W, to nearly 10% of train speed. The magnitude of V and W increases the overall magnitude on average by ~10% above of the longitudinal velocity component U, higher than previously observed and above the Cobra probe lower range of data acceptance (Gil et al., 2008).

4. Discussion

It is possible to analyse results by splitting the flow into a number of key flow regions, each with different characteristics. A more detailed analysis of U within these specific regions is

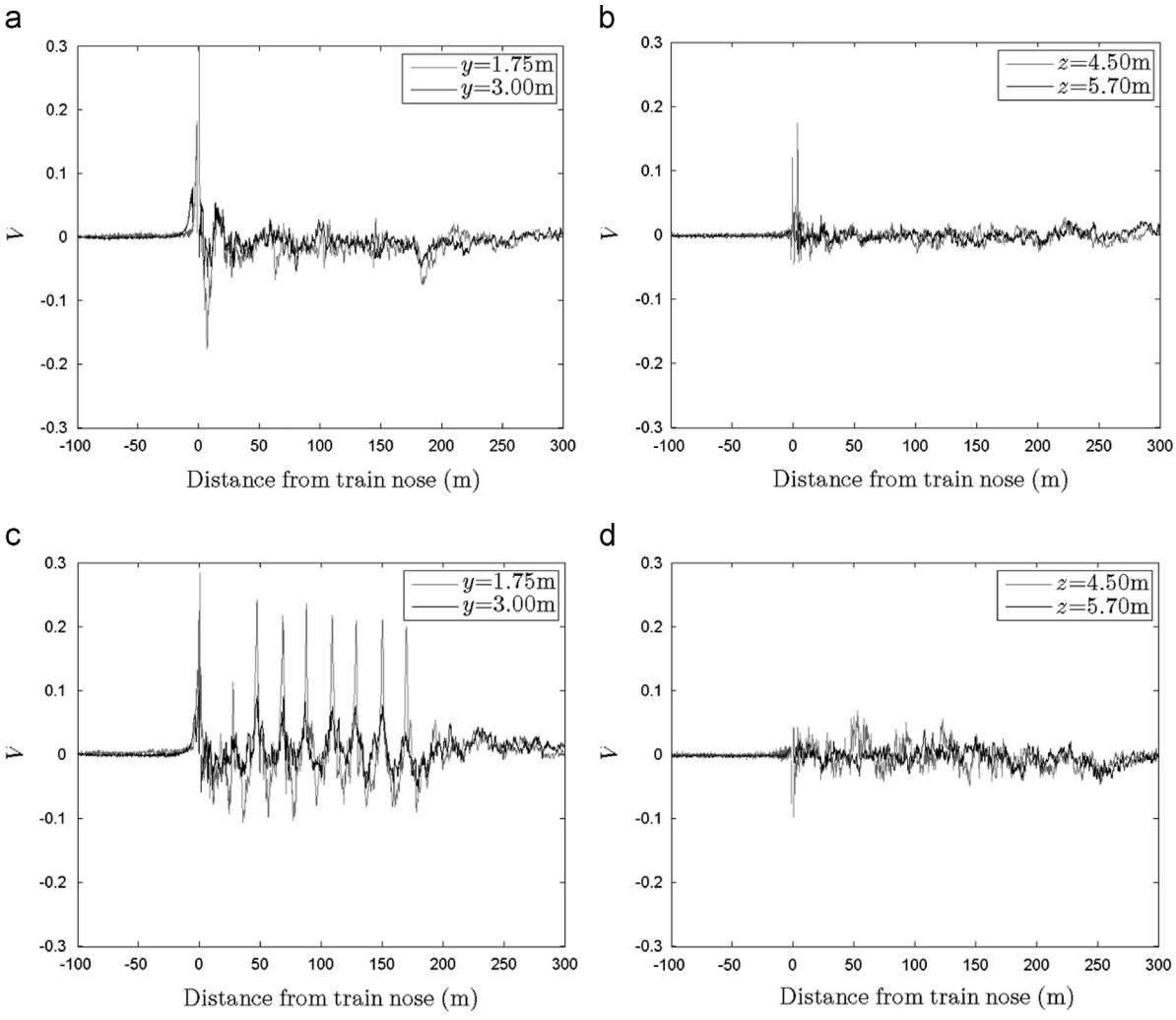

Fig. 11. The normalised ensemble lateral component of velocity V for the 8 wagon train with freight consists 1 and 3. Measurements are made at train side at a height of $z=2.25$ m at distances $y=1.75$ m and $y=3$ m from the centre of track, and above the train roof for heights $z=4.5$ m and $z=5.7$ m at a position of 0 m from the centre of track. a) Consist 1 probes 1 and 2; b) Consist 1 probes 3 and 4; c) Consist 3 probes 1 and 2 and d) Consist 3 probes 3 and 4.

undertaken using a variety of analysis techniques to understand the varying flow nature.

Previous model- and full-scale studies (Baker et al., 2001; Sterling et al., 2008) suggest the nose velocity peak is highly reproducible. In Section 3.2 the reproducibility of the nose peak has again been highlighted, however a similar analysis as presented in Baker et al. (2013), using inviscid potential flow theory to model the nose peak through an application of Bernoulli's equation, does not provide a

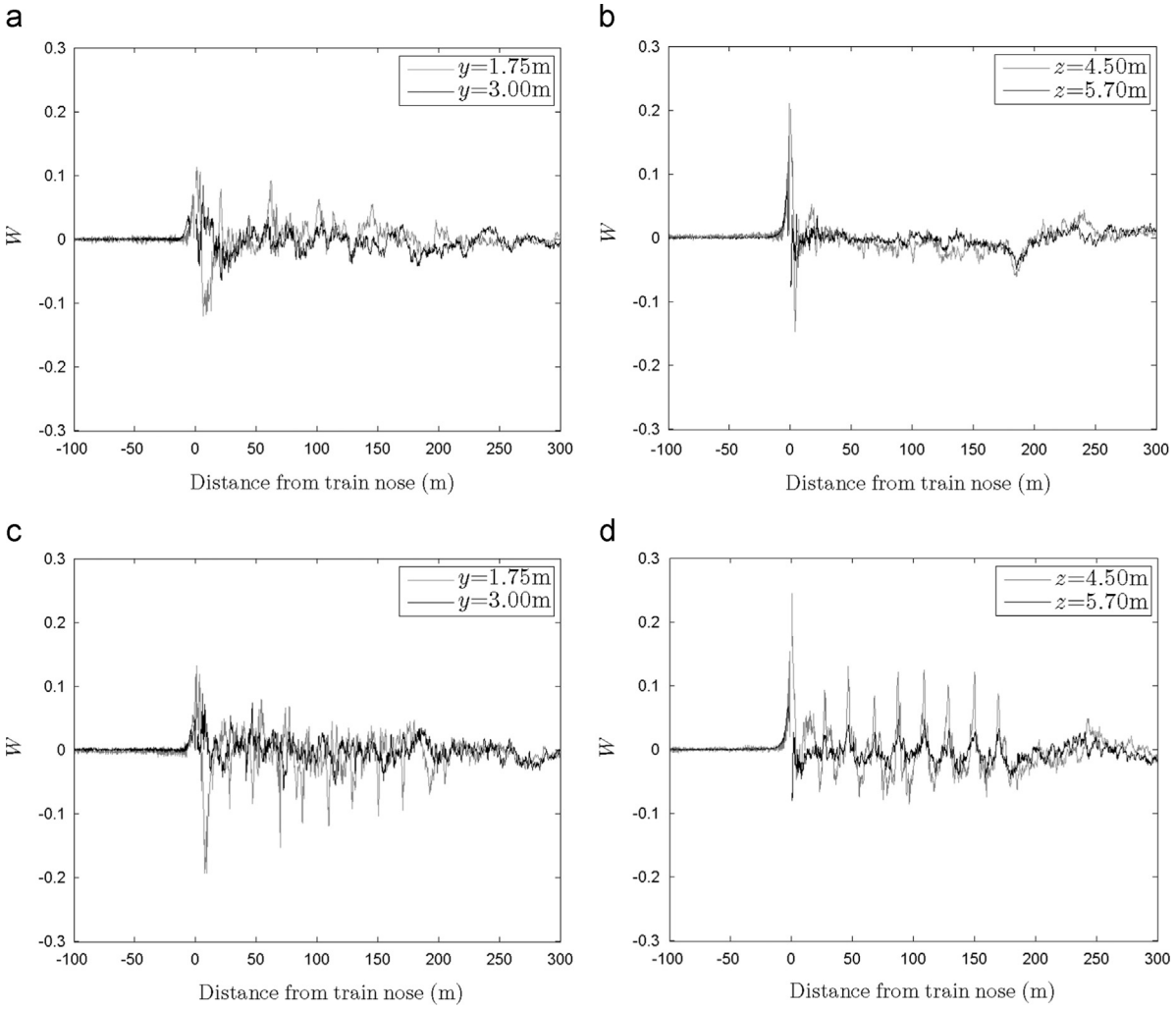

Fig. 12. The normalised ensemble vertical component of velocity W for the 8 wagon train with freight consists 1 and 3. Measurements are made at train side at a height of $z=2.25$ m at distances $y=1.75$ m and $y=3$ m from the centre of track, and above the train roof for heights $z=4.5$ m and $z=5.7$ m at a position of 0 m from the centre of track a) Consist 1 probes 1 and 2; b) Consist 1 probes 3 and 4; c) Consist 3 probes 1 and 2 and d) Consist 3 probes 3 and 4.

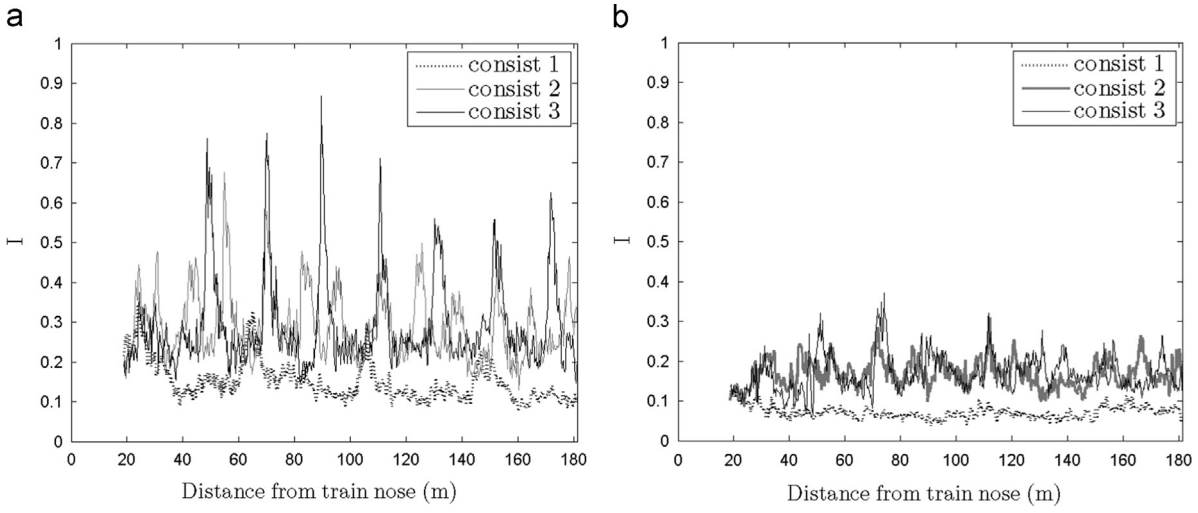

Fig. 13. Turbulence intensities for the 8 wagon train with freight consists 1, 2 and 3. Measurements are made at train side at a height of $z=2.25$ m at distance $y=1.75$ m from the centre of track and above the train roof at a height of $z=4.5$ m and a distance of $y=0$ m from the centre of track. a) Probe 1 and b) Probe 3.

characteristic equation for the nose peak associated with the Class 66. Potential flow theory analysis presumes a high speed passenger train to have a smooth rounded nose shape, which the Class 66 does not have.

Sterling et al. (2008) suggested full-scale container freight data with a nose peak time scale of 0.2 s based on train speed 33 m/s, could potentially cause passenger instability; however it was concluded that the relatively small magnitude (~25%) was unlikely to create this problem. In this study, close to the train side (1.75 m from the centre of track (probe 1)), a nose peak of magnitude 120% in U extending 10 m has been found. For a train speed $V_{train}=20$ m/s the 10 m peak extents relate to a time scale of 0.5 s, beyond the suggested range to create passenger instability (Sterling et al., 2008; Jordan et al., 2009). However, at full UK freight speed of 33.5 m/s this relates to a time scale of 0.3 s, which coupled with a peak magnitude of 120% could potentially cause passenger instability.

Within the boundary layer region ($18.75\ \text{m} \le x \le 181.25$ m (train end)) a series of analysis including velocity profiles, displacement thickness, turbulence intensity and autocorrelations have been carried out. Results show clear differences are observed between container loading efficiencies and in general results exhibit higher magnitudes than observed in previous passenger studies. As the analysis techniques are based on U, it is clear that reducing container loading efficiency increases slipstream velocities, creating pulse peaks at the leading face of loaded containers. This in turn creates a thicker boundary layer with an increasing displacement thickness, with large pulse increases and fluctuations in relation to loading configurations. The turbulence intensity is defined as the ratio of the standard deviation of the ensemble velocity to one minus the ensemble mean, defined for a moving frame of reference with respect to the train. Fig. 13 clearly indicates that as the container loading efficiency is reduced regions of higher turbulence intensity occur at the lead face of a loaded container. Autocorrelation results, shown in Fig. 14, indicate that much of the energy within the boundary layer region is at time scales below 0.5 s, i.e. high levels of small scale turbulence, as witnessed in full-scale container freight data (Sterling et al., 2008). Correlations above the train roof exhibit a periodic oscillation of frequency 10–20 Hz, thought to be related to a periodic flow separation from the leading edge of the Class 66 roof at the nose. A useful property of correlograms is the integral under the curve represents the integral time scale (Kundu and Cohen, 2010). By taking a discrete integral (trapezium method) under the average autocorrelation from the zero lag to the first zero crossing it is possible to find the integral time scale for each consist, and thus multiplying by train speed an integral length scale. The results are shown in Table 2, note all integral time and length scales are given in relation to an equivalent full-scale train.

For all consists the integral time scales are shorter than 0.35 s and integral length scales range from 3 m to 7 m. The influence of spaces between containers not only creates larger turbulent scales, during processes such as flow separation at container lead faces, but also higher levels of small turbulent scales within the boundary layer. This is reflected by shorter integral time and length scales for poorly loaded consists 2 and 3 in relation to consist 1. Sterling et al. (2008) stated that time scales less than 0.1 s with a length scale between 3 and 5 m are too rapid for the human body to react and are unlikely to cause human instability. However, for a partially loaded consist with a repeated loading configuration there are repeating gusts within a timescale that could lead to human instability. If the results are scaled to full UK freight line speed of 33.5 m/s this creates an average time scale of 0.2 s with a length scale between 5 and 9.5 m, within the suggested range likely to cause human instability (Sterling et al., 2008; Jordan et al., 2009).

In the tail region, boundary layer growth ceases and U falls away into the wake, at a similar rate for all consists. In previous passenger studies a large tail velocity peak is witnessed due to longitudinal helical vortices; however as discussed this is not observed for the freight train. Intuitively it is suggested research into flow around surface mounted cuboids in a line should provide the closest

Table 2
Autocorrelation integral time and length scales for freight consists 1 to 3 at probe positions 1 to 3. Measurements are made at train side at a height of $z=2.25$ m at distances $y=1.75$ m and $y=3$ m from the centre of track, and above the train roof for height $z=4.5$ m at a position of 0 m from the centre of track.

Probe number		Consist number		
		1	2	3
1	Time scale (s)	0.20	0.16	0.16
	Length scale (m)	4.10	3.19	3.21
2	Time scale (s)	0.35	0.28	0.23
	Length scale (m)	7.09	5.57	4.67
3	Time scale (s)	0.24	0.18	0.18
	Length scale (m)	4.83	3.57	3.60

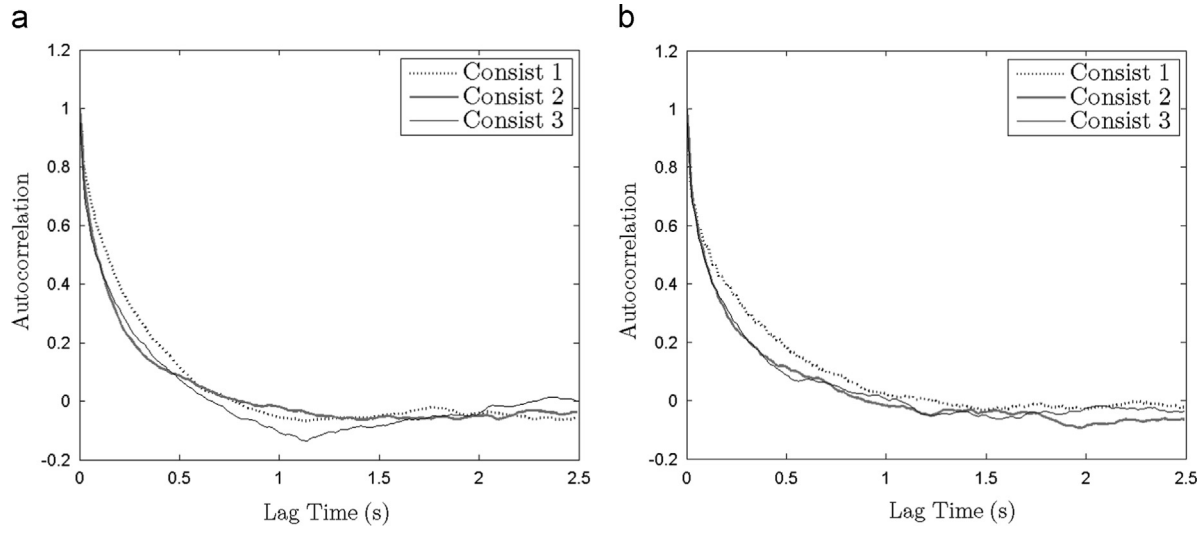

Fig. 14. Correlograms to show autocorrelation for the 8 wagon train with freight consists 1, 2 and 3. Measurements are made at train side at a height of $z=2.25$ m at distance $y=1.75$ m from the centre of track and above the train roof at a height of $z=4.5$ m and a distance of $y=0$ m from the centre of track. a) Probe 1 and b) Probe3.

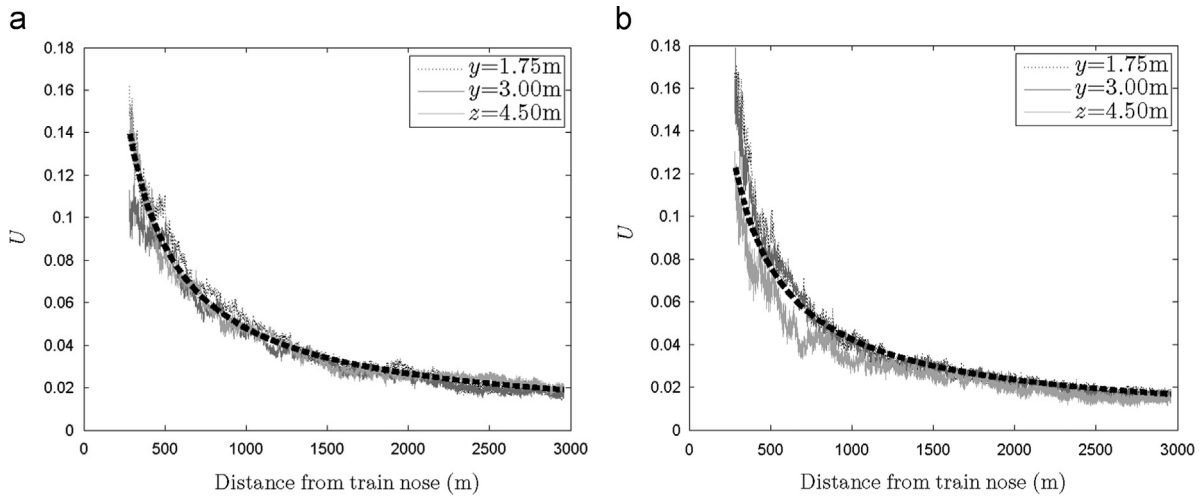

Fig. 15. The far wake region (100 m from the train end) for the normalised ensemble longitudinal component of velocity U for train consists 1 and 3. The dashed black line indicates the fitted curve by the power law with q set to -0.85. Measurements are made at train side at a height of $z=2.25$ m at distances $y=1.75$ m and $y=3$ m from the centre of track, and above the train roof at a height of $z=4.5$ m at a distance $y=0$ m from the centre of track. (a) Consist 1 and (b) Consist 3.

comparison for a container freight train. At the rear face of a surface mounted cuboid a recirculation zone is observed for flows with a similar Reynolds number to the model freight train at the TRAIN rig, however the zone extends remain relatively bounded by the cuboid rear face edges (Stoesser et al., 2003). It is suggested that contrary to a passenger train with shedding vortices, a container freight train is more likely to have a recirculation zone in the tail region. At the train tail there is a negative peak in V at train side and a negative peak in W above the train roof at 10 m beyond the train end, suggesting a recirculation bubble closely bounded to the rear of the last container. However, due to Cobra probe positioning and sampling capability it is suggested that it will not be possible to fully observe this recirculation at the TRAIN rig. A numerical simulation through the application of CFD focusing on the rear of a container freight train is most likely to highlight characteristic flow patterns in this region.

Baker et al. (2013) discusses similarity of velocity decay in the far wake region between different passenger train types. By modelling velocity decay using a power law type equation,

$$U = a(x)^q \tag{5}$$

where x is the longitudinal position of the train, Baker et al. (2013) found for passenger trains a common power of $q=-0.5$ could be applied. Using the definition from Baker et al. (2013) that the far wake is taken to occur at distances greater than 100 m from the end of the train, a common power of $q=-0.85$ has been calculated for the freight train. Fig. 15 shows the decay of U in the far wake for consists 1 and 3 for the 8 wagon train plotted with the fitted power law curve. The curve fit generally exhibits good agreement with the far wake data for all consists. It is expected that differences between passenger and freight train common powers occur because of differences in shape between train tails, with freight trains lacking any aerodynamic features found on passenger trains. Passenger trains are generally self-contained vehicles which can be driven from both ends, thus the nose and tail features are in most cases the same, unlike a freight train hauled by a locomotive at the front. (a) Consist 1 and (b) Consist 3.

5. Conclusions

For the first time, a thorough analysis of the slipstreams associated with a freight train has been undertaken at model-scale. The results show a number of important findings,

(1) It is possible to present slipstream results as a series of flow regions as in previous passenger studies, albeit with differing flow development with these specific regions. Compared with typical passenger train velocity and pressure magnitudes large differences are found in the nose and tail regions, related to vehicle shape. Velocity and pressure magnitudes in the nose region are much larger than any values observed in train slipstream studies previously.
(2) Clear differences in slipstream development are observed for differing container loading configurations.
   (a) For C_p, as loading efficiencies are decreased, a series of positive then negative peaks are observed about the lead face of loaded containers, the magnitude of which is dependent on space size between loaded containers.
   (b) As loading efficiencies are decreased the magnitude of velocities within the boundary layer are increased, with a series of pulse peaks relating to the change in pressure at the lead face of loaded containers.
   (c) For loading efficiencies of more than 50% boundary layer growth stabilises rapidly within the first four wagon lengths. However, for loading efficiencies of less than 50% continual boundary layer growth is observed until after five wagon lengths when boundary layer stabilisation occurs.
   (d) Velocities in the lateral and vertical directions have magnitudes much larger than previously observed in passenger studies; increasing the overall magnitude by $\sim$10%. A series of pulse peaks are observed in V and W at the lead face of containers as loading efficiencies are decreased. Flow directions in the nose region suggest a flow reversal emanating from the leading edges of the Class 66 nose. Similarly flow directions in the tail region suggest a recirculation zone following the final loaded container.
   (e) Magnitudes of velocities and pressure above the train roof are smaller than magnitudes recorded at a similar distance from the train surface at the train side. For all cases as the distance from the train surface is increased velocity and pressure magnitudes decrease.
(3) A series of in-depth analysis has been undertaken in each of the flow regions identified. Analysis has highlighted differences created through decreased loading efficiencies, creating increased boundary layer growth with a larger displacement thickness with higher turbulence intensities.
(4) Autocorrelation analysis highlighted a possible vortex shedding emanating from the leading edge of the Class 66 nose

above the roof. Integral time and length scales calculated through autocorrelation highlighted that limits of human instability, calculated by Sterling et al. (2008), are exceeded for the container freight train with a lower loading efficiency.

(5) In the far wake, as discussed in Baker et al. (2013), there is a large degree of similarity between velocity decay in the wake for all consists. It is possible to express the decay in terms of a power law with a common power.

Acknowledgements

The authors would like to thank Dr Sarah Jordan, Dr Francesco Dorigatti, Dr Timothy Gilbert and Martin Gallagher from the University of Birmingham, for their help with performing the moving model experiments. The work was financed by a University of Birmingham funded scholarship.

References

Department for Transport DfT. Delivering a Sustainable Railway. In: TRANSPORT, D. F. (Ed.), 2007.

Woodburn, A., 2008. An investigation of container train service provision and load factors in Great Britain. Eur J Transp Infrastruct Res 11 (3), 147–165.

Frost, M.W., Ison, S.G., Watson., R., 2012. UK rail transport: a review of demand and supply. Proc. ICE—Transp. 165 (3), 225–234.

Baker, C.J., Dalley, S.J., Johnson, T., Quinn, A.D., Wright., N.G., 2001. The slipstream and wake of a high speed train. Proc. Inst. Mech. Eng. Part F J. Rail Rapid Transit 215, 83–99.

Temple, J., Johnson, T., Effective Management of Risk from Slipstream Effects at Trackside and on Platforms. Technical Report, A Report Produced for Rail Safety and Standards Board, August 2008.

Baker, C.J., Quinn, A., Sima, M., Hoefener, L., Licciardello, R., 2013. Full-scale measurement and analysis of train slipstreams and wakes: Part 1 ensemble averages. Proc. Inst. Mech. Eng. Part F J. Rail Rapid Transit, 1–17.

Pope, C., Safety of Slipstreams Effects Produced by Trains. A Report Prepared by Mott Macdonald Ltd for RSSB, 2006.

Sterling, M., Baker, C.J., Jordan, S.C., Johnson, T., 2008. A study of the slipstreams of high speed passenger trains and freight trains. Proc. Inst. Mech. Eng. Part F J. Rail Rapid Transit 222 (177-19).

Technical Specifications for Interoperability. Commission Decision of 21 February 2008 Concerning the Technical Specification for Interoperability Relating to the Rolling Stock Subsystem of the Trans-European High-speed Rail System. Technical Report, Official Journal of the European Union, 2008.

Soper, D. The Aerodynamics of a Container Freight Train. Ph.D. Thesis, University of Birmingham, 2014.

Baker, C.J., Jordan, S., Gilbert, T., Quinn, A.D., Sterling, M., Johnson, T., Lane., J., 2014. Transient aerodynamic pressures and forces on trackside and overhead structures due to passing trains. Part 1: Model-scale experiments; Part 2: Standards applications. Proc. Inst. Mech. Eng. Part F J. Rail Rapid Transit 228 (no. 1), 37–70.

Dorigatti, F. Rail Vehicles in Crosswinds: Analysis of Steady and Unsteady Aerodynamic Effects Through Static and Moving Model Tests. Ph.D. Thesis, University of Birmingham, 2013.

Soper, D., C. Baker, M. Sterling. Assessing crosswind effects on a container freight train with differing container loading configurations. In: First International Conference in Numerical and Experimental Aerodynamics of Road Vehicles and Trains, Bordeaux, France., 2014.

Alam, F., S. Watkins. Effects of crosswinds on double stacked container wagons. In: 16th Australasian Fluid Mechanics Conference, December 3–7, Gold Coast, Australia, 2007.

Hemida, H., Baker, C., 2010. Large-eddy simulation of the flow around a freight wagon subjected to a crosswind. Comput. Fluids 39 (10), 1944–1956.

Baker, C.J., 2010. The flow around high speed trains. J. Wind Eng. Ind. Aerodyn. 98, 277–298.

Muld, T., Slipstream and Flow Structures in the Near-Wake of High-Speed Trains. Ph.D. Thesis. KTH Royal Institute of Technology, Stockholm, Sweden, 2012.

Gil, N., Baker, C., Roberts., C., 2008. The measurement of train slipstream characteristics using a rotating rail rig. In: Sixth Int. Colloq. on Bluff Body Aerodynamics and its Applications.

TFI, Turbulent flow instrumentation – Cobra Probe – Getting Started Guide, 2011.

Hemida, H., Gil, N., Baker, C., 2010. LES of the slipstream of a rotating train. J. Fluids Eng. 132.

Jordan, S., Sterling, M., Baker, C., 2009. Modelling the response of a standing person to the slipstream generated by a passenger train. Proc. Inst. Mech. Eng. Part F J. Rail Rapid Transit 223 (6), 567–579 (6).

Kundu, P.K., Cohen, I.M., 2010. Fluid Mechanics. Academic Press, San Diego, CA.

Stoesser, T., Mathey, F., Frohlich, J., Rodi, W., 2003. Les of flow over multiple cubes. Ercoftac Bull. 56, 15–19.